Electronic Supporting Information

Synthesis and characterization of two self-assembled $[Cu_6Gd_3]$ and $[Cu_5Dy_2]$ complexes exhibiting magnetocaloric effect, slow relaxation of magnetization and anticancer activity

Avik Bhanja[a], Sangeeta Roy Chaudhuri[a], Angelos B. Canaj,[b] Shachi Pranjal Vyas,[c] Fabrizio Ortu[d], Lucy Smythe,[b] Mark Murrie,[b] Ritobrata Goswami,[c] Debashis Ray*[a]

[a]*Department of Chemistry, Indian Institute of Technology, Kharagpur 721302, India*
[b]*School of Chemistry, University of Glasgow, University Avenue, Glasgow, G12 8QQ, UK*
[c]*School of Bioscience, Indian Institute of Technology, Kharagpur 721302, India*
[d]*School of Chemistry, University of Leicester, LE1 7RH Leicester, UK*

**Email: dray@chem.iitkgp.ac.in*

Contents

Experimental Section

Materials. Solvents and other laboratory grade reagents used in this work were either as obtained or purified according to standard literature procedure.[S1] *o*-vanillin (Spectrochem Pvt Ltd, Mumbai), $DyCl_3 \cdot 6H_2O$ and $GdCl_3 \cdot 6H_2O$ (Alfa Aesar, India), 2-amino-2-methylpropan-1-ol (Alfa Aesar, India) and triethylamine (S D Fine Chemicals, Mumbai, India) were used as received without further purification. $Cu(ClO_4)_2 \cdot 6H_2O$ was obtained by treating an aqueous perchloric acid (1:1) with commercial $CuCO_3$, followed by concentration and crystallization on a water bath. Human serum albumin (fatty acid free, fraction V) was obtained from Sigma-Aldrich (USA). Calf thymus DNA (*ct*-DNA), ethidium bromide (EB) and dimethyl sulfoxide (DMSO) were purchased from Sisco Research Laboratories (Mumbai, India). Dulbecco's Modified Eagle medium (DMEM), Dulbecco's Modified Eagle Medium High glucose (DMEM-high glucose) and Dulbecco's Modified Eagle medium: Nutrient mixture F12 (DMEM/F-12), Dulbecco's phosphate buffered saline (PBS), Foetal Bovine Serum (FBS), 0.25% trypsin-EDTA and antibiotic-antimycotic solution were procured from Thermo Fisher Scientific (MA, USA). MTT (3-4,5-dimethyl-2-thiazolyl)-2,5-diphenyl-2H-tetrazolium bromide was obtained from HiMedia (Mumbai, India). Solutions of complexes **1** and **2** were prepared in DMSO and subsequent dilutions were made with buffers (pH 7.4) during biochemical studies.

Caution! Metal complexes of organic ligands with perchlorate counterions are potentially explosive in nature in dry state. Therefore, the material should be prepared in very small amount, and it should be handled with extreme care.

Physical Measurements. The absorption spectra were collected using a Shimadzu (Model UV2450) spectrophotometer. Elemental analysis (C, H, N) of the complex were performed with a Perkin-Elmer model 240C elemental analyser. IR measurements were recorded using KBr disks in a Perkin-Elmer FT-IR spectrometer model RX1. The purity of the bulk complex were measured by powder XRD using a BRUKER AXS X-ray diffractometer (40 kV, 20 mA) using Cu-Kα radiation (λ = 1.5418 Å) within 5–50° (2θ) range and a fixed-time counting of 4 s at 25°C. The steady-state fluorescence spectra were recorded with a Horiba Jobin Yvon spectrofluorometer (Flurolog-3) equipped with temperature-controlled water-cooled cuvette holder and a 1 cm path length quartz cuvette was used to take the scan of the solutions. All magnetic measurements were carried out on powdered crystalline samples restrained in eicosane using a Quantum Design SQUID magnetometer (MPMS-XL or MPMS 3). Data were

corrected for the diamagnetic contribution of the sample holder and eicosane by measurements, and for the diamagnetism of each compound. Thermogravimetric analysis (TGA) was carried out by using a PerkinElmer Pyris Diamond TG-DTA instrument.

X-ray Crystallography. Appropriate single crystals of **1** and **2** was chosen for data collection on a Bruker SMART APEX-II CCD X-ray diffractometer furnished with a graphite-monochromated Mo Kα ($\lambda = 0.71073$ Å) radiation by the ω scan (width of 0.3° frame^{-1}) method at 293 K with a scan rate of 6 s per frame. Data processing and space group determination were done by SAINT and XPREP software's.[S2] The crystal structures were solved by direct method technique from SHELXS-2014[S3] and then refined by full-matrix least squares technique using SHELXL (2014/7)[S4] program packaged within WINGX version 1.80.05.[S5] Multiscan empirical absorption corrections were applied to the data using the program SADABS.[S6] The locations of the heaviest atoms i.e. Cu and Dy were determined easily and the O, N, and C atoms were subsequently determined from the difference Fourier maps. The other non-hydrogen atoms were refined with anisotropic displacement parameters. Hydrogen atoms were fixed at calculated positions, and their positions were refined by a riding model. Due to the disorders, the lattice solvent molecules of both the complexes cannot be modelled satisfactorily. So, the Olex-2 software having the mask program[S7] suite has been performed to discard those disordered solvent molecules and gave electron density of 75 and 207 respectively. This value allowed us to assign four and twenty H_2O molecules for complexes **1** and **2** respectively. From the % weight loss of thermogravimetric analysis, we have got 2.68% loss for complex **1** and 14.17% loss for complex **2** which is equivalent to 4 H_2O and 21 H_2O respectively (Fig. S9). Crystallographic Figures presented in this manuscript were generated using DIAMOND software.[S8] The crystal data and the cell parameters for compounds **1**−**2** are summarized in Table S2 in the ESI. Crystallographic data (excluding structure factors) have been deposited with the Cambridge Crystallographic Data Centre as supplementary publications CCDC 2184365 and 2184368. These data can also be obtained free of cost at www.ccdc.cam.ac.uk/conts/retrieving.html (or from the Cambridge Crystallographic Data Centre).

Synthesis of 2-[(2-hydroxy-1,1-dimethyl-ethylimino)-methyl]-6-methoxy-phenol (H_2L)

H_2L was obtained from Schiff base condensation reaction between the chosen aldehyde and its amine counterpart. To a stirred solution of 2-amino-2-methylpropan-1-ol (0.18 g, 2 mmol) in MeOH (10 mL) was added 10 mL MeOH solution of 2-hydroxy-3-methoxybenzaldehyde (0.30 g, 2 mmol) in 1:1 molar ratio. After complete addition, the solution was allowed to stir for 30

min followed by a reflux of 2 h duration. Then the whole solution was evaporated under reduced pressure to reduce the solvent volume to obtain an orange oily mass. Repeated washing was made with *n*-hexane to remove the unreacted reactants and finally the substance was dried under vacuum over P_4O_{10}. The oily substance was characterized by FTIR and NMR spectroscopy, and use directly in complex formation reaction without any other purification process such as column chromatography. FT-IR (KBr) cm^{-1}: 3360 (br), 1630 (s), 1505 (m), 1469 (w), 1366 (w), 1219 (s), 1168 (m), 1063 (m), 856 (w). ^1H NMR (400 MHz, $CDCl_3$, ppm): 8.23 (1H, imine H), 6.82 (2H, ArH), 6.62 (1H, ArH), 3.82 (3H. methoxy H), 3.57 (2H, methyne H), 1.30 (6H, methyl H).

General Procedure for Synthesizing 1–2. A general and reproducible reaction protocol was used for the synthesis of **1** and **2** at room temperature under magnetic stirring conditions. H_2L (0.22 g; 0.1 mmol) was dissolved into 10 mL of MeOH-$CHCl_3$ (2:1, v/v) solvent mixture and solid $Cu(ClO_4)_2 \cdot 6H_2O$ (0.1 mmol, 0.31 g) was added into it followed by addition of NEt_3 (0.2 g, 0.2 mmol) as base giving a bright green solution. After stirring for 1 h, solid $LnCl_3 \cdot 5H_2O$ (0.05 mmol) (Ln = Dy^{3+}, Gd^{3+}) was added to the previous solution when the whole solution turned into bluish-green. The resulting solution was finally stirred for overnight at room temperature, filtered and kept for slow evaporation in air. After a week, green block-shaped single crystals suitable for X-ray diffraction analysis were obtained. The quantity of reactants involved in each case and characterization data of the products are given below.

$[Cu_6Gd_3(L)_3(HL)_3(\mu_3\text{-}Cl)_3(\mu_3\text{-}OH)_6(OH)_2]ClO_4 \cdot 4H_2O$ (**1**). Yield: 0.022 g, 50.09 % (based on Gd^{3+}). FT-IR (KBr) cm^{-1}: 3493 (br), 2967 (w), 2671 (w), 1641(s), 1613 (m), 1456 (s), 1389 (m), 1297 (m), 1245 (s), 1219 (s), 1088 (s), 967 (m), 737 (m), 619 (w) Anal. Calcd. for $C_{72}H_{108}Cl_4Cu_6Gd_3N_6O_{34}$ (2596.48): C, 33.31; H, 4.19; N, 3.24. Found: C, 33.37; H, 4.17; N, 3.26.

$[Cu_5Dy_2(L)_2(HL)_2(\mu\text{-}Cl)_2(\mu_3\text{-}OH)_4(ClO_4)_2(H_2O)_6](ClO_4)_2 \cdot 2NHEt_3Cl \cdot 21H_2O$ (**2**). Yield: 0.028 g, 39.60 % (based on Dy^{3+}). FT-IR (KBr) cm^{-1}: 3497 (br), 2971 (w), 2679 (w), 1643(s), 1609 (m), 1458 (s), 1395 (m), 1295 (m), 1242 (s), 1224 (s), 1090 (s), 965 (m), 743 (m), 621 (w) Anal. Calcd. for $C_{60}H_{152}Cl_8Cu_5Dy_2N_6O_{59}$ (2828.22): C, 25.48; H, 5.42; N, 2.97. Found: C, 25.51; H, 5.41; N, 2.95.

Cell culture

Human lung adenocarcinoma cell line (A549), human breast cancer cell line (MDA-MB-231) were obtained from National Centre for Cell Science (Pune, India) and human embryonic kidney cell line (HEK 293T) was a generous gift from Dr Arindam Mondal, School of

Bioscience, IIT Kharagpur. A549, MDA-MB-231 and HEK 293T were grown in DMEM/F12, DMEM-high glucose and DMEM media, respectively with 10% FBS and 1% antibiotic-antimycotic in a humidified atmosphere at 37ºC temperature and 5% CO_2.

Cytotoxicity assessment

The cytotoxicity of the synthesized copper complexes was determined in cancerous (A549 and MDA-MB-231) and normal (HEK 293T) cell line using MTT assay. It is based on the reduction of the MTT reagent into insoluble formazan crystals by the mitochondrial dehydrogenases of the viable cells. The insoluble formazan crystals are then solubilised by an organic solvent such as DMSO and the purple formazan product thus formed is measured by a multi-well plate reader (1). Briefly, 1×10^4 cells/well were seeded in a 96-well plate overnight at 37^0C. Thereafter, cells were treated with different copper complexes at a range of concentrations (**1**: 5, 15, 30, 45 and 60 μM), (**2**, SM1, SM2 and SM3: 10, 25, 50, 75 and 100 μM) for 24 hrs. Next, the media containing the copper complexes was decanted and the cells were washed with PBS followed by incubation with 100 μL MTT (5 mg/mL) for 3 hrs. Later, MTT solution was discarded and the insoluble formazan crystals thus formed were solubilised by adding 100 μL of DMSO in each well. The purple formazan crystals were then measured using spectrophotometer at 590 nm.

***In vitro* DNA binding studies**

The experiments involving the interactions of the synthesized complexes **1** and **2** with *ct*-DNA were performed in Tris–HCl buffer (5mM Tris-HCl, 50 mM NaCl, pH 7.2) at room temperature. Purity of the used *ct*-DNA in the working buffer was evaluated from the ratio of absorbance at 260 to 280 nm, which was found to be >1.8, indicating the DNA is sufficiently free from protein. The concentration of the *ct*-DNA per nucleotide was calculated from the absorbance band at 260 nm using the molar extinction coefficient (ε = 6600 M^{-1} cm^{-1}).[S9]

Absorption spectroscopic studies

Absorption titration experiments of each complex were carried out in Shimadzu 1800 spectrometer with the addition of an increasing amount of *ct*-DNA (0–50 μM) in Tris-HCl buffer (pH 7.2) to a fixed concentration of the metal complex (23 μM). Equal quantities of *ct*-DNA were added to the reference solution during each titration to eliminate the effect of *ct* -DNA absorption. From the absorption data, the intrinsic binding constant K_a was obtained following the Benesi–Hildebrand approach using eqn (S1).[S10]

$$\frac{1}{\Delta A} = \frac{1}{(\varepsilon_b - \varepsilon_f)L_T} + \frac{1}{(\varepsilon_b - \varepsilon_f)L_T K_a} \cdot \frac{1}{M} \qquad (S1)$$

Here, ε_b and ε_f are the extinction coefficients (charge transfer band) of the synthesized complex in fully bound form and of the free complex, respectively, for a particular DNA concentration, M. L_T is the total complex concentration and ΔA is the change in the absorbance at a given wavelength. By plotting the reciprocal of ΔA versus the reciprocal of concentration of *ct*-DNA, the association constant (K_a) can be obtained from the ratio of the intercept to the slope.

Fluorescence Quenching

To assess the magnitude of interaction quantitatively, the quenching efficiency was evaluated using the Stern–Volmer equation

$$\frac{I_0}{I} = 1 + K_{SV} r \qquad (S2)$$

Where I_0 and I are the emission intensities in absence and presence of the complexes respectively, K_{sv} is the Stern−Volmer quenching constant and r is the concentration of the quencher (complex). From the linear plot of I_o/I *vs*. [complex]/[DNA], the quenching constant K_{sv} can be calculated from the ratio of the slope to the intercept.

Fluorescence binding study

Emission intensity measurements were carried out using a Horiba Jobin Yvon spectrofluorometer (Flurolog-3) fluorescence spectrophotometer at room temperature. Luminescence titration quenching experiments were conducted by adding aliquots of of *ct*-DNA (0 to 32 μM DNA) to fixed concentration of complexes **1** and **2** (25 μM) in Tris-HCl buffer.

The relative binding of the ternary complexes to *ct* DNA was studied by fluorescence spectral method using ethidium bromide (EB) bound *ct* DNA solution in Tris–HCl/NaCl buffer (pH, 7.2) following a previously reported literature method. Subsequent addition of complexes **1** and **2** with increasing concentration (0–33 μM) quenched the fluorescence of the EB-DNA adduct. Based on fluorescence quenching, apparent binding constant (K_{app}) was calculated from the equation (S3)

$$[EB] \times K_{EB} = [complex]_{50\%} \times K_{app}, \qquad (S3)$$

Where, [EB] denotes the concentration of ethidium bromide and $[complex]_{50\%}$ is the concentration that is required to quench the fluorescence of the EB-DNA adduct by 50% (K_{EB} = 1.0 × 10^7 M^{-1}, [EB] = 3.5 μM).

HSA Binding Studies

In this study quenching of tryptophan fluorescence has been monitored using human serum albumin (HSA, 2 μM) in 10 mM phosphate buffer (pH 7.4) in Horiba Jobin Yvon spectrofluorometer (Flurolog-3). The fluorescence emission spectra of the Trp residue of HSA were recorded at room temperature by setting the excitation wavelength at 295 nm and the scan range of 305–445 nm. Fluorometric titration experiments were carried out by using 3 mL solutions of 2 μM HSA with successive addition of **1** and **2** from the concentration range of 0 to 8.8 μM. Each spectrum was corrected with respect to the corresponding blank.

Determination of the fluorescence quenching process has been obtained from Stern–Volmer using eqn S4

$$\frac{F_0}{F} = 1 + K_{SV}[Q] \qquad (S4)$$

Here F_0 and F are the unquenched-to-quenched fluorescence intensities in the absence and presence of the *3d-4f* quencher complexes, respectively, [Q] is the concentration of the quencher and K_{SV} is the Stern–Volmer constant. K_{SV} is related to both the fluorescence lifetime of the fluorophore and the rate constant for the quenching process (eqn S5).

$$K_{SV} = k_q \tau_0 \qquad (S5)$$

Here τ_0 is the lifetime of the unquenched fluorophore (5 ns) and k_q is the bimolecular quenching constant.[S11] The quenching constant, also known as the binding constant K_a, and the number of binding sites (n) between the albumin protein and metal ion complexes were calculated using the Scatchard equation S6.[S12]

$$log\frac{F_0 - F}{F} = \log K_a + nlog[Q] \quad (S6)$$

The binding constant (K_a) for the formation of adducts between the *3d-4f* complexes or {*3d-4f*} fragments and HSA was determined using the double logarithmic plots (Fig. S16 c and f). The values of K_{SV} and n for complexes **1** and **2** are summarized in Table 4 in manuscript.

Table S1. Representative Examples of Cu^{II}/Gd^{III} Complexes having Magnetocaloric properties

Compounds[a]	Experimental ΔS_m($J{\cdot}kg^{-1}{\cdot}K^{-1}$)	Theoretical ΔS_m($J{\cdot}kg^{-1}{\cdot}K^{-1}$)	Ref.
$[Gd_2Cu_6(Gly)_6(FA)_3(\mu_3\text{-}OH)_3(\mu_3\text{-}OH_2)_3(H_2O)_9](ClO_4)_6$	6.0	28.7	S13
$[Gd_2Cu_6(Gly)_6(FA)_3(\mu_3\text{ -}OH)_3(\mu_3\text{-}OH_2)_3(H_2O)_8]$	5.8	30.1	S13
$[Gd_4Cu_8(OH)_8(Me_3CCOO)_8(hmp)_8](NO_3)_2(OH)_2$	13.5	32.6	S14
$[\{Cu_5Gd_2(L^1)_2(\mu_3\text{-}OH)_4(NO_3)_4(\mu\text{-}OH_2)_2\}(NO_3)_2]_n$	15.7	34.37	S15
$[Gd_2Cu_6(ipo)_6(H_2O)_{12}]$	13.97	34.8	S16
$[\{Gd(hfac)_3\}_3\{Cu(hfac)\}\{NIT\text{–}Ph(OMe)_2\}_4]_n$	13.5	20.24	S17
$[Cu_6Gd_2(L^2)_6(L^2H)_6(MeOH)_6]_n$	11.8	22.62	S18
$[Cu_5Gd_4O_2(OMe)_4(teaH)_4(O_2CC(CH_3)_3)_2(NO_3)_4]$	31	34.93	S19
$[Cu_4Gd_{12}(OH)_{20}(teaH)_2(teaH_2)_4(O_2CPh\text{-}2\text{-}Ph)_8(H_2O)_6Cl_2](Cl)_6$	33.0	42.1	S20
$Na[Cu_{24}Gd_6(L\text{-}Ala)_{12}(Ac)_6(\mu_3\text{-}OH)_{30}(NO_3)_4(H_2O)_{20}](NO_3)_8(OH)_7$	21.2	39.1	S21
$[Gd_4Cu_8(OH)_8(hmp)_8(O_2CCHMe_2)_8](ClO_4)_4$	14.6	23.02	S22
$[Cu_4Gd_2(OH)_2(NO_3)_8\{(py)_2CO_2\}_2(MeCN)_4]$	22.9	34.9	S23
$[\{(Cu(salen)\}_2Gd(NO_3)_3]$	17	24.4	S24

[a]FA: Formic acid; Gly: Glycine; L^1H_3: N,N' -bis-(3-methoxysalicylidene)-1,3-diamino-2-propanol; ipoH3: 2-hydroxy-isophthalic acid; NIT–Ph$(OMe)_2$: 2-(2,4-dimethoxyphenyl)-4,4,5,5-tetramethyl-imidazolyl-1-oxyl-3-oxide; hfac: hexafluoroacetyl acetone; L^2H2: acenaphthenequinone dioxime; $teaH_3$: triethanolamine; Hhmp: 2-pyridinylmethanol.

Table S2 Crystal data and refinement parameter of **1** and **2**

parameters	**1**	**2**
Formula	$C_{72}H_{108}Cl_4Cu_6Gd_3N_6O_{34}$	$C_{60}H_{152}Cl_8Cu_5Dy_2N_6O_{59}$
F.W.(g mol^{-1})	2596.48	2828.17
crystal system	monoclinic	triclinic
space group	P 21/c	P −1
Crystal color	Green	Green
Crystal size/mm^3	0.2×0.1×0.01	0.28×0.13×0.11
limiting indices	−26 ≤ h ≤ 26 −48 ≤ k ≤ 48 −26 ≤ l ≤ 32	−18 ≤ h ≤ 17 −18 ≤ k ≤ 18 −19 ≤ l ≤ 16
a/ Å	21.5095(5)	14.468(15)
b/ Å	39.1997(8)	15.061(13)
c/ Å	26.0609(4)	15.723(14)
α/ deg	90	87.63(9)
β/ deg	96.3670(16)	68.21(7)
γ/ deg	90	69.24(7)
V/ $Å^3$	21838.1(7)	2959(5)
D_c/g cm^{-3}	1.536	1.587

μ (mm^{-1})	3.102	2.398
F(000)	9984	1239
θ for data collection (deg)	1.562 – 26.372	2.858 – 26.420
T/K	150	299(2)
Total reflns	199345	34495
R(int)	0.1116	0.0649
Unique reflns	44429	11918
Observed reflns	24988	8261
Parameters	2267	526
R_1; wR_2 ($I > 2\sigma(I)$)	0.0793, 0.2254	0.0467, 0.1178
GOF (F^2)	1.052	1.086
Largest diff peak and hole (e Å^{-3})	1.899, -1.265	0.863, -0.935
CCDC No.	2184365	2184368

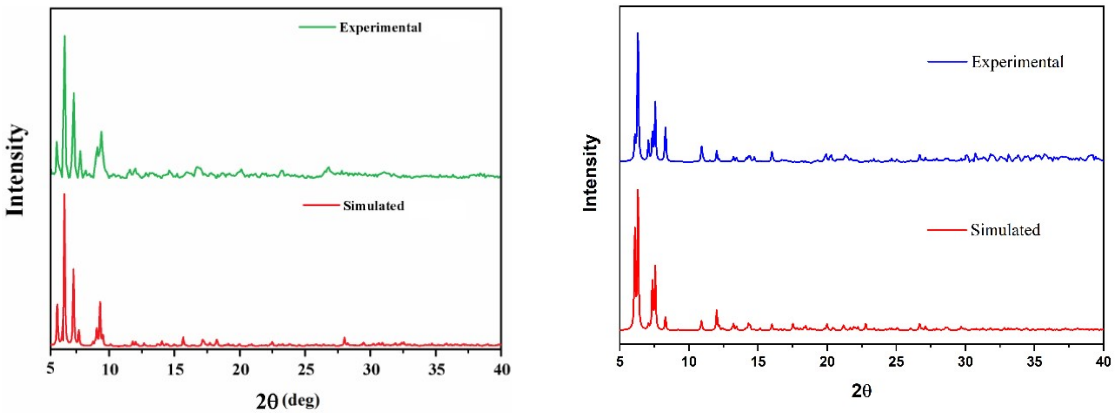

Fig. S1 Powder XRD pattern of Cu_6Gd_3 (**1**) and Cu_5Dy_2 (**2**) complexes

Chart S1. Ligand with available pockets and observed coordination mode of H_2L[S25]

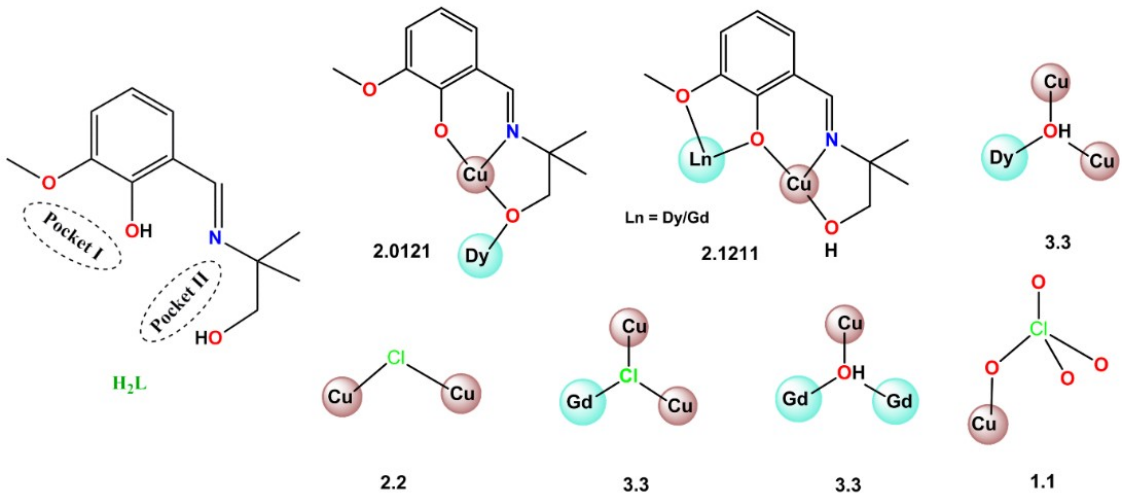

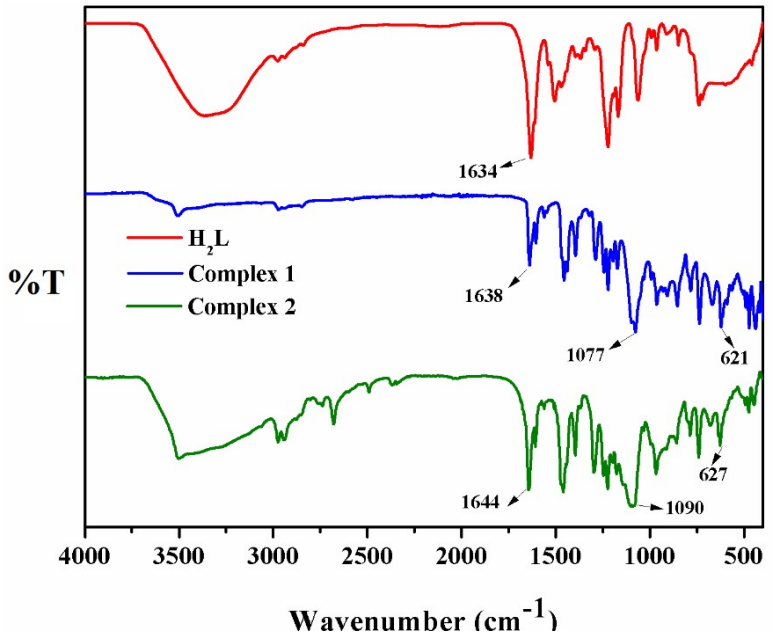

Fig. S2 FTIR spectra of H_2L, complex **1** and complex **2**

Table S3 Results of continuous shape measures calculations[S26–S27] using program SHAPE 2.1 for Cu^{II} atoms of **1** and **2**.[a]

[ML5]	PP-5	vOC-5	TBPY-5	**SPY-5**	JTBPY-5
Cu1 of **1**	30.075	3.577	5.725	**1.933**	9.957
Cu1 of **2**	28.796	2.788	6.761	**2.331**	10.345
Cu2 of **2**	30.698	3.529	4.688	**1.657**	8.855

[a]*PP-5 = Pentagon, vOC-5 = Vacant octahedron, TBPY-5 = Trigonal bipyramid, SPY-5 = Spherical square pyramid, JTBPY-5 = Johnson trigonal bipyramid J12*

Table S4 Results of continuous shape measures calculations[S26–S27] using program SHAPE 2.1 for Cu3 atoms of **2**.[a]

	JPPY-6	TPR-6	**OC-6**	PPY-6	HP-6
Cu3 of **2**	31.098	17.203	**2.503**	28.836	30.935

[a]*JPPY-6 = Johnson pentagonal pyramid J2, TPR-6 = Trigonal prism, OC-6 = Octahedron, PPY-6 = Pentagonal pyramid, HP-6 = Hexagon*

Table S5 Results of continuous shape measures calculations[S26–S27] using program SHAPE 2.1 for Gd1 atoms of **1**.[a]

[ML10]	DP-10	EPY-10	OBPY-10	PPR-10	PAPR-10	JBCCU-10	JBCSAPR-10	JMBIC-10	JATDI-10	**JSPC-10**	SDD-10	TD-10	HD-10
Gd1 of **1**	36.438	24.642	17.071	10.108	14.676	13.468	5.245	10.395	19.638	**1.837**	6.833	6.156	11.440

Gd3 of **1**	36.494	24.806	16.994	10.275	14.607	13.297	4.804	9.940	19.580	**1.789**	6.630	5.896	11.303

[a]*DP-10 = Decagon, EPY-10 = Enneagonal pyramid, OBPY-10 = Octagonal bipyramid, PPR-10 = Pentagonal prism, PAPR-10 = Pentagonal antiprism, JBCCU-10 = Bicapped cube J15, JBCSAPR-10 = Bicapped square antiprism J17, JMBIC-10 = Metabidiminished icosahedron J62, JATDI-10 = Augmented tridiminished icosahedron J64, JSPC-10 = Sphenocorona J87, SDD-10 = Staggered Dodecahedron, TD-10 = Tetradecahedron, HD-10 = Hexadecahedron*

Table S6 Results of continuous shape measures calculations[S26–S27] using program SHAPE 2.1 for Gd2 atoms of **1**.[a]

[ML9]	EP-9	OPY-9	HBPY-9	JTC-9	JCCU-9	CCU-9	JCSAPR-9	CSAPR-9	**JTCTPR-9**	TCTPR-9	JTDIC-9	HH-9	MFF-9
Gd2 of **1**	38.062	21.716	22.295	16.410	10.665	10.873	1.964	2.313	**0.935**	1.431	11.225	14.793	3.161

[a]*EP-9 = Enneagon, OPY-9 = Octagonal pyramid, HBPY-9 = Heptagonal bipyramid, JTC-9 = Johnson triangular cupola J3, JCCU-9 = Capped cube J8, CCU-9 = Spherical-relaxed capped cube, JCSAPR-9 = Capped square antiprism J10, CSAPR-9 = Spherical capped square antiprism, JTCTPR-9 = Tricapped trigonal prism J51, TCTPR-9 = Spherical tricapped trigonal prism, JTDIC-9 = Tridiminished icosahedron J63, HH-9 = Hula-hoop, MFF-9 = Muffin*

Table S7 Results of continuous shape measures calculations[S26–S27] using program SHAPE 2.1 for Dy1 atoms of **1**.[a]

[ML8]	OP-8	HPY-8	HBPY-8	CU-8	SAPR-8	**TDD-8**	JGBF-8	JETBPY-8	JBTPR-8	BTPR-8	JSD-8	TT-8
Dy1 of **2**	33.578	20.476	14.352	11.331	4.388	**2.569**	11.725	24.915	2.575	2.406	4.765	11.866

[a]*OP-8 = Octagon, HPY-8 = Heptagonal pyramid, HBPY-8 = Hexagonal bipyramid, CU-8 = Cube, SAPR-8 = square antiprism, TDD-8 = Triangular dodecahedron, JGBF-8 = Johnson gyrobifastigium J26, JETBPY-8 = Johnson elongated triangular bipyramid J14, JBTPR-8 = Biaugmented trigonal prism J50, BTPR-8 = Biaugmented trigonal prism, JSD-8 = Snub diphenoid J84, TT-8 = Triakis tetrahedron*

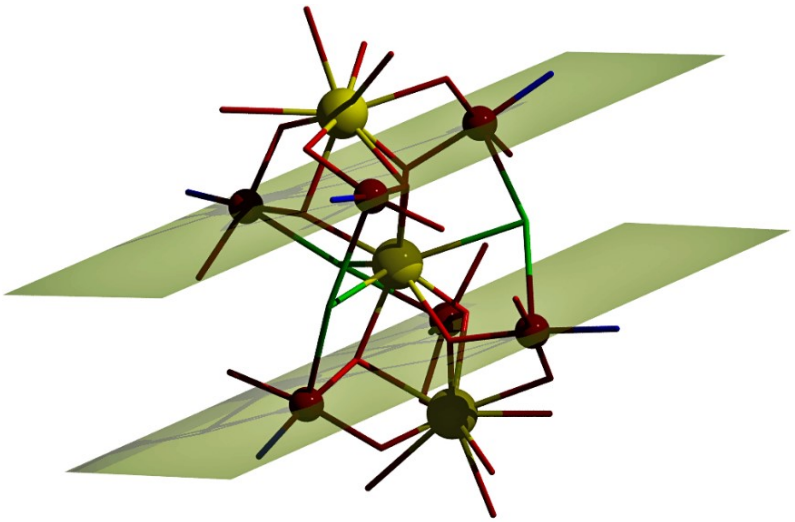

Fig. S3 Two Cu_3 unit containing parallel planes present in complex **1**

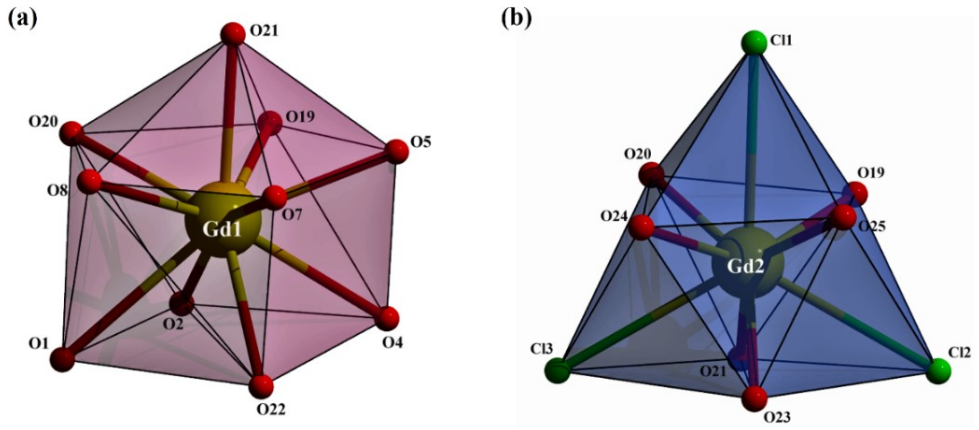

Fig. S4 (a) Distorted sphenocorona geometry around Gd1; (b) distorted tricapped trigonal prismatic geometry around Gd2.

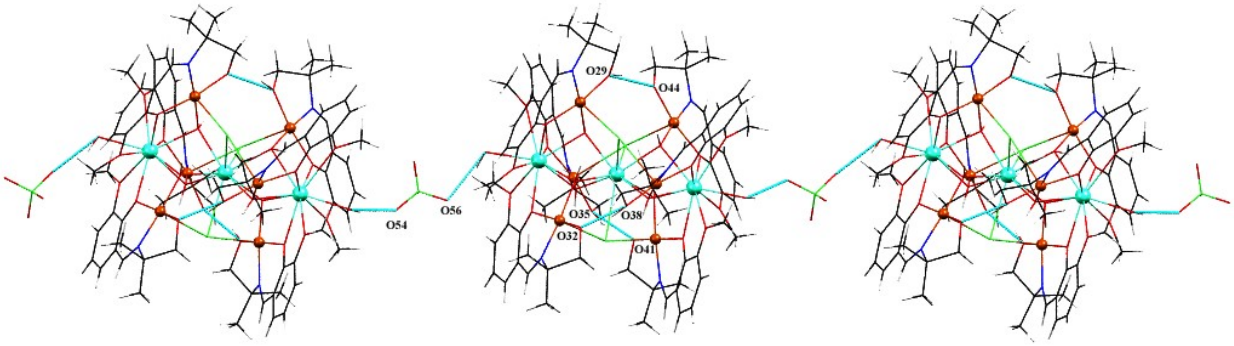

Fig. S5 1D-chain like H-bonding present in complex **1** through perchlorate anion.

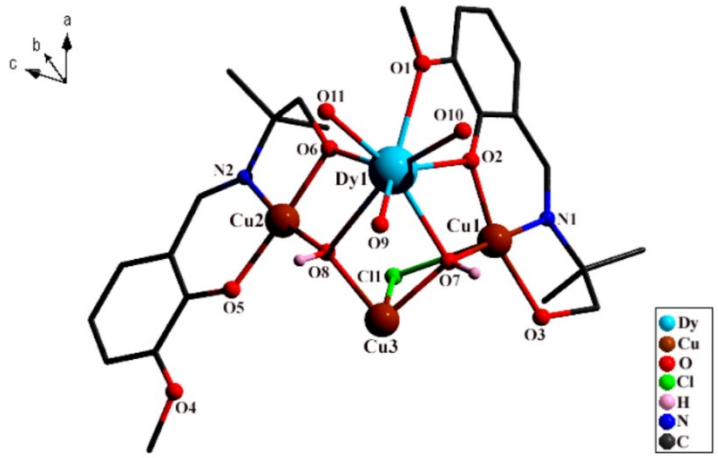

Fig. S6 Asymmetric unit of **2** with partial atom numbering. Counter anion and solvent molecules are omitted for clarity.

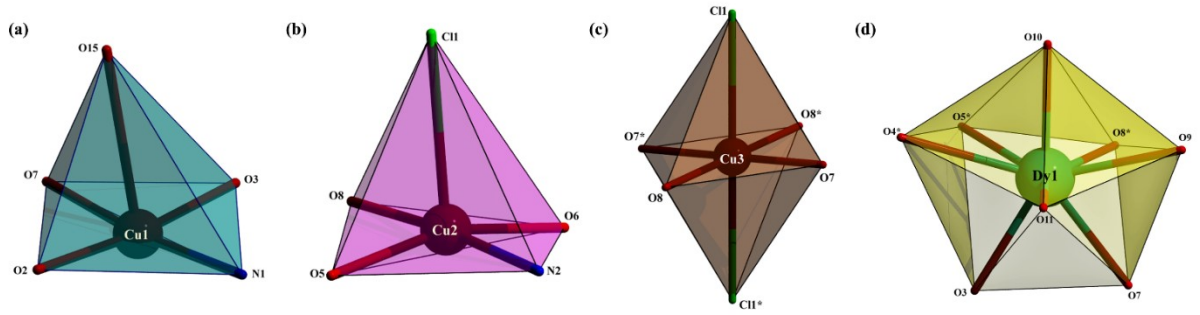

Fig. S7 Coordination environments around metal ion centers (a) Cu1: distorted square pyramidal; (b) Cu2: distorted square pyramidal (c) Cu3: distorted octahedral and (d) Dy1: distorted biaugmented trigonal prism geometry.

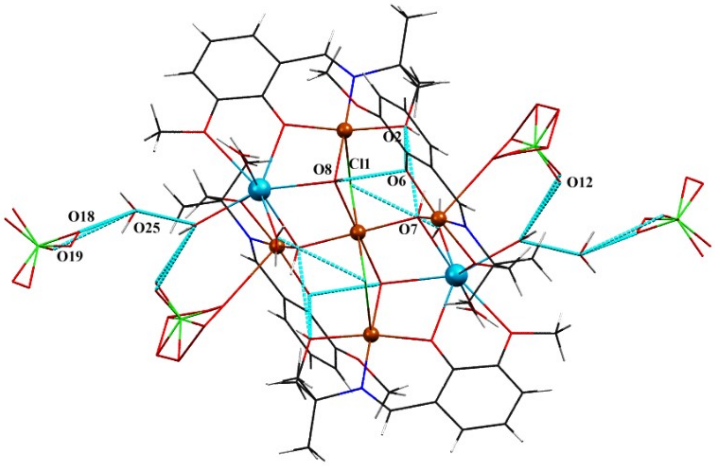

Fig. S8 Weak intra-molecular hydrogen bonding present in complex **2**. Solvent molecules are omitted for clarity.

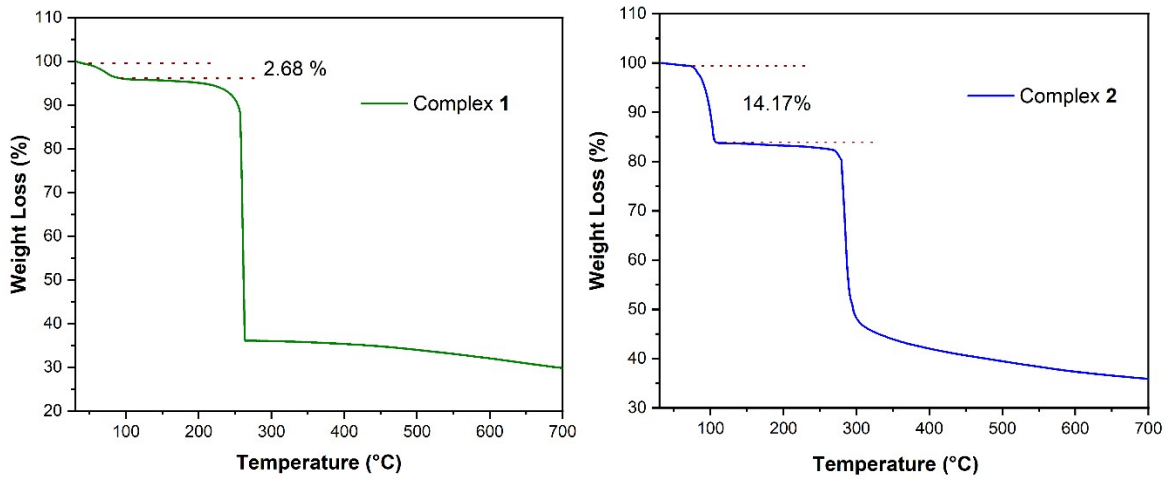

Fig. S9 TGA curves of complexes **1** and **2**. The % of weight loss in the temperature range 70−110 ºC is: **1**; 2.68 and **2**; 14.17.

Table S8 Selected bond distances of **1**

Atom 1	Atom 2	Distance [Å]		Atom 1	Atom 2	Distance [Å]
Gd1	O1	2.764(7)		Gd3	O25	2.447(7)
Gd1	O2	2.431(7)		Gd3	O26	2.450(8)
Gd1	O4	2.705(7)		Cu1	O2	1.959(7)
Gd1	O5	2.424(7)		Cu1	O3	1.926(7)
Gd1	O7	2.689(7)		Cu1	O19	1.918(7)
Gd1	O8	2.400(7)		Cu1	N1	1.941(9)
Gd1	O19	2.422(7)		Cu2	O5	1.961(7)
Gd1	O20	2.426(7)		Cu2	O6	1.923(7)
Gd1	O21	2.435(6)		Cu2	O21	1.925(7)
Gd1	O22	2.457(7)		Cu2	N2	1.955(8)
Gd2	Cl1	3.023(3)		Cu3	O8	1.926(7)
Gd2	Cl2	2.997(2)		Cu3	O9	1.950(7)
Gd2	Cl3	3.000(2)		Cu3	O20	1.923(7)
Gd2	O19	2.384(7)		Cu3	N3	1.933(9)
Gd2	O20	2.393(7)		Cu4	O11	1.942(7)
Gd2	O21	2.379(6)		Cu4	O12	1.936(7)
Gd2	O23	2.385(7)		Cu4	O23	1.936(6)
Gd2	O24	2.364(7)		Cu4	N4	1.923(9)
Gd2	O25	2.405(6)		Cu5	O14	1.940(7)
Gd3	O10	2.778(8)		Cu5	O15	1.922(7)
Gd3	O11	2.406(7)		Cu5	O24	1.923(6)
Gd3	O13	2.705(7)		Cu5	N5	1.913(9)
Gd3	O14	2.429(7)		Cu6	O17	1.938(7)
Gd3	O16	2.713(7)		Cu6	O18	1.935(7)
Gd3	O17	2.415(7)		Cu6	O25	1.912(6)
Gd3	O23	2.417(7)		Cu6	N6	1.926(8)
Gd3	O24	2.448(6)				

Table S9 Selected bond angles of **1**

Atom 1	Atom 2	Atom 3	Bond Angles(°)		Atom 1	Atom 2	Atom 3	Bond Angles(°)
O2	Gd1	O1	59.6(2)		O19	Gd1	O20	70.2(2)
O2	Gd1	O4	67.1(2)		O19	Gd1	O21	69.0(2)
O2	Gd1	O7	159.3(2)		O19	Gd1	O22	139.0(2)
O2	Gd1	O21	128.1(2)		O20	Gd1	O1	70.8(2)
O2	Gd1	O22	91.2(2)		O20	Gd1	O2	72.7(2)
O4	Gd1	O1	104.9(2)		O20	Gd1	O4	134.3(2)
O5	Gd1	O1	159.9(2)		O20	Gd1	O7	120.8(2)
O5	Gd1	O2	118.0(2)		O20	Gd1	O21	70.5(2)
O5	Gd1	O4	59.7(2)		O20	Gd1	O22	136.3(2)
O5	Gd1	O7	67.6(2)		O21	Gd1	O1	133.8(2)
O5	Gd1	O20	128.9(2)		O21	Gd1	O4	120.1(2)
O5	Gd1	O21	64.9(2)		O21	Gd1	O7	72.7(2)
O5	Gd1	O22	94.7(2)		O21	Gd1	O22	140.4(2)
O7	Gd1	O1	107.7(2)		O22	Gd1	O1	66.1(2)
O7	Gd1	O4	104.1(2)		O22	Gd1	O4	66.3(2)
O8	Gd1	O1	67.9(2)		O22	Gd1	O7	68.1(3)
O8	Gd1	O2	120.3(2)		Cl2	Gd2	Cl1	118.24(7)
O8	Gd1	O4	158.0(2)		Cl2	Gd2	Cl3	120.22(7)
O8	Gd1	O5	121.0(2)		Cl3	Gd2	Cl1	121.54(7)
O8	Gd1	O7	61.3(2)		O19	Gd2	Cl1	72.48(18)
O8	Gd1	O19	128.3(2)		O19	Gd2	Cl2	67.57(17)
O8	Gd1	O20	64.6(2)		O19	Gd2	Cl2	131.55(17)
O8	Gd1	O21	73.3(2)		O19	Gd2	O20	71.4(2)
O8	Gd1	O22	92.2(2)		O19	Gd2	O23	135.4(2)
O19	Gd1	O1	118.8(2)		O19	Gd2	O25	96.8(2)
O19	Gd1	O2	64.8(2)		O20	Gd2	Cl1	67.79(17)
O19	Gd1	O4	73.6(2)		O20	Gd2	Cl2	132.93(18)
O19	Gd1	O5	71.5(2)		O20	Gd2	Cl3	73.19(18)
O19	Gd1	O7	132.6(2)		O20	Gd2	O25	134.9(2)

O21	Gd2	Cl1	131.95(16)		O11	Gd3	O25	129.3(2)
O21	Gd2	Cl2	73.34(17)		O11	Gd3	O26	91.0(3)
O21	Gd2	Cl3	67.71(17)		O13	Gd3	O10	107.5(2)
O21	Gd2	O19	70.6(2)		O13	Gd3	O16	102.6(2)
O21	Gd2	O20	72.0(2)		O14	Gd3	O10	67.9(2)
O21	Gd2	O23	95.6(2)		O14	Gd3	O13	60.6(2)
O21	Gd2	O25	146.3(2)		O14	Gd3	O16	158.2(2)
O23	Gd2	Cl1	132.46(17)		O14	Gd3	O24	65.2(2)
O23	Gd2	Cl2	67.85(17)		O14	Gd3	O25	71.4(2)
O23	Gd2	Cl3	72.76(17)		O14	Gd3	O26	90.9(3)
O23	Gd2	O20	145.9(2)		O16	Gd3	O10	108.5(2)
O23	Gd2	O25	71.3(2)		O17	Gd3	O10	163.7(2)
O24	Gd2	Cl1	72.77(16)		O17	Gd3	O13	66.6(2)
O24	Gd2	Cl2	133.19(16)		O17	Gd3	O14	117.6(2)
O24	Gd2	Cl3	68.25(16)		O17	Gd3	O16	60.3(2)
O24	Gd2	O19	145.2(2)		O17	Gd3	O23	71.2(2)
O24	Gd2	O20	93.9(2)		O17	Gd3	O24	126.6(2)
O24	Gd2	O21	135.9(2)		O17	Gd3	O25	63.6(2)
O24	Gd2	O25	71.0(2)		O23	Gd3	O10	118.5(2)
O25	Gd2	Cl1	67.14(16)		O23	Gd3	O13	133.1(2)
O25	Gd2	Cl2	73.00(16)		O23	Gd3	O14	129.2(2)
O25	Gd2	Cl3	131.68(17)		O23	Gd3	O16	72.1(2)
O11	Gd3	O10	59.7(2)		O23	Gd3	O24	70.9(2)
O11	Gd3	O13	157.1(2)		O23	Gd3	O25	70.0(2)
O11	Gd3	O14	122.0(2)		O23	Gd3	O26	139.6(3)
O11	Gd3	O16	67.8(2)		O24	Gd3	O10	69.6(2)
O11	Gd3	O17	119.8(2)		O24	Gd3	O13	121.1(2)
O11	Gd3	O23	65.5(2)		O24	Gd3	O16	135.2(2)
O11	Gd3	O24	74.4(2)		O24	Gd3	O26	136.3(3)
O25	Gd3	O10	130.8(2)		N4	Cu4	O12	86.1(4)
O25	Gd3	O13	73.6(2)		N4	Cu4	O23	175.5(4)
O25	Gd3	O16	119.4(2)		O15	Cu5	O14	169.6(3)

O25	Gd3	O24	69.0(2)		O15	Cu5	O24	97.0(3)
O25	Gd3	O26	139.6(3)		O24	Cu5	O14	85.7(3)
O26	Gd3	O10	67.6(3)		N5	Cu5	O14	91.6(3)
O26	Gd3	O13	66.1(3)		N5	Cu5	O15	85.3(4)
O26	Gd3	O16	68.6(3)		N5	Cu5	O24	176.9(4)
O3	Cu1	O2	169.5(3)		O18	Cu6	O17	169.4(3)
O3	Cu1	N1	85.6(3)		O25	Cu6	O17	83.5(3)
O19	Cu1	O2	84.2(3)		O25	Cu6	O18	97.4(3)
O19	Cu1	O3	97.0(3)		O25	Cu6	N6	175.5(3)
O19	Cu1	N1	175.3(3)		N6	Cu6	O17	92.8(3)
N1	Cu1	O2	92.5(3)		N6	Cu6	O18	85.8(3)
O6	Cu2	O5	171.2(3)		Cu1	O2	Gd1	104.0(3)
O6	Cu2	O21	97.8(3)		Cu3	O8	Gd1	105.7(3)
O6	Cu2	N2	85.1(3)		Cu4	O11	Gd3	104.3(3)
O21	Cu2	O5	84.3(3)		Cu5	O14	Gd3	103.9(3)
O21	Cu2	N2	174.8(3)		Cu6	O17	Gd3	106.0(3)
N2	Cu2	O5	92.3(3)		Gd2	O19	Gd1	96.4(2)
O8	Cu3	O9	169.4(3)		Cu1	O19	Gd1	105.6(3)
O8	Cu3	N3	93.4(4)		Cu1	O19	Gd2	122.2(3)
O20	Cu3	O8	84.1(3)		Gd2	O20	Gd1	96.1(2)
O20	Cu3	O9	98.1(3)		Cu3	O20	Gd1	104.8(3)
O20	Cu3	N3	175.7(4)		Cu3	O20	Gd2	120.2(3)
N3	Cu3	O9	83.6(4)		Gd2	O21	Gd1	96.2(2)
O12	Cu4	O11	169.2(3)		Cu2	O21	Gd1	105.2(3)
O23	Cu4	O11	84.5(3)		Cu2	O21	Gd2	121.9(3)
O23	Cu4	O12	96.3(3)		Gd2	O23	Gd3	96.5(2)
N4	Cu4	O11	92.3(4)		Cu4	O23	Gd2	122.7(3)
Cu4	O23	Gd3	104.0(3)		Cu5	O24	Gd3	103.8(3)
Gd2	O24	Gd3	96.2(2)		Gd2	O25	Gd3	95.2(2)
Cu5	O24	Gd2	123.1(3)					

Table S10 Selected bond distances of **2**

Atom 1	Atom 2	Distance [Å]		Atom 1	Atom 2	Distance [Å]
Dy1	O7	2.381(3)		Cu3	Cl1	2.684(3)
Dy1	O8	2.407(5)		Cu3	Cl1	2.684(3)
Dy1	O5	2.316(4)		Cu2	O8	1.951(4)
Dy1	O3	2.219(4)		Cu2	O5	1.919(4)
Dy1	O4	2.578(4)		Cu2	O6	1.987(4)
Dy1	O9	2.427(4)		Cu2	N2	1.931(5)
Dy1	O10	2.366(4)		Cu2	Cl1	2.695(3)
Dy1	O11	2.334(5)		Cu1	O7	1.973(4)
Cu3	O7	1.969(4)		Cu1	O2	1.919(3)
Cu3	O7	1.969(4)		Cu1	O3	1.935(4)
Cu3	O8	2.005(3)		Cu1	N1	1.920(4)
Cu3	O8	2.005(3)				

Table S11 Selected bond angles of **2**

Atom 1	Atom 2	Atom 3	Bond Angles(°)		Atom 1	Atom 2	Atom 3	Bond Angles(°)
O7	Dy1	O8*	67.87(14)		O2	Cu1	N1	95.83(17)
O7	Dy1	O4*	144.58(12)		O3	Cu1	O7	84.52(15)
O7	Dy1	O9	71.97(13)		N1	Cu1	O7	170.83(14)
O8	Dy1*	O4	127.82(14)		N1	Cu1	O3	86.37(17)
O8*	Dy1	O9	76.19(15)		O8	Cu2	O6	94.85(16) .
O5*	Dy1	O7	113.60(13)		O8	Cu2	Cl1	84.53(11)
O5	Dy1*	O8	66.65(13)		O5	Cu2	O8	84.23(15) .
O5	Dy1*	O4	62.32(14)		O5	Cu2	O6	161.26(15)
O5*	Dy1	O9	134.89(16)		O5	Cu2	N2	94.79(18)
O5*	Dy1	O10	85.69(15)		O5	Cu2	Cl1	99.21(14)
O5*	Dy1	O11	140.20(13)		O6	Cu2	Cl1	99.33(14)
O3	Dy1	O7	69.57(12)		N2	Cu2	O8	174.17(16)
O3	Dy1	O8*	113.15(14)		N2	Cu2	O6	84.22(18)
O3	Dy1	O5*	87.21(15)		N2	Cu2	Cl1	101.30(15)

O3	Dy1	O4*	75.03(13)		O7	Cu3	O7*	180
O3	Dy1	O9	132.04(15)		O7	Cu3	O8*	84.53(16)
O3	Dy1	O10	145.22(14)		O7	Cu3	O8	95.47(16)
O3	Dy1	O11	82.16(17)		O7	Cu3	Cl1*	87.35(13)
O9	Dy1	O4*	138.09(13)		O7	Cu3	Cl1	92.65(13)
O10	Dy1	O7	143.47(13)		O8	Cu3	O8*	180
O10	Dy1	O8*	95.01(16)		O8	Cu3	Cl1*	96.16(11)
O10	Dy1	O4*	71.52(15)		O8	Cu3	Cl1	83.84(11)
O10	Dy1	O9	72.67(15)		Cl1	Cu3	Cl1*	180
O11	Dy1	O7	98.34(16)		Cu3	O7	Cu1	115.72(17)
O11	Dy1	O8*	151.83(13)		Cu1	O7	Dy1	99.30(13)
O11	Dy1	O4*	77.87(17)		Cu3	O8	Dy1*	102.68(16)
O11	Dy1	O9	76.16(18)		Cu2	O8	Dy1*	100.81(14)
O11	Dy1	O10	81.80(17)		Cu2	O8	Cu3	110.79(16)
O2	Cu1	O7	93.12(14)		Cu2	O5	Dy1*	105.10(15)
O2	Cu1	O3	173.63(15)		Cu1	O3	Dy1	106.28(15)

Table S12 Intra-molecular hydrogen bonding interactions present in complex **2**

Interactions	**D─H (Å)**	**D···A (Å)**	**H···A (Å)**	**D─H···A (º)**
O6−H6···O2	0.865	2.667	1.973	136.46
O6−H6···O7	0.865	2.907	2.729	93.10
O9−H9A···Cl1	0.93	3.131	2.868	97.66
O9−H9B···Cl5	0.93	3.085	2.717	104.54
O10−H10B···Cl5	0.93	3.112	2.873	96.09
O11−H11A···O12	0.93	2.843	2.005	148.98
O11−H11B···O25	0.93	2.685	1.976	133.57

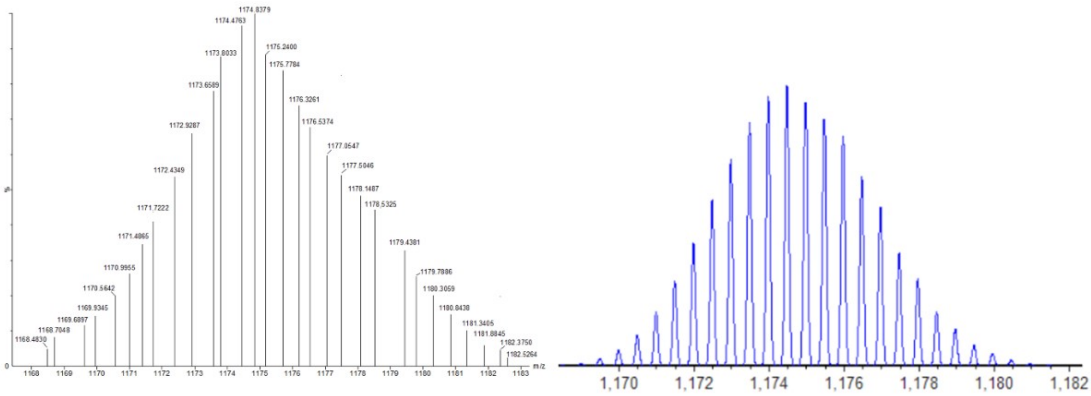

Fig. S10 Simulated and experimental isotope pattern of the prominent peak for $[C_{72}H_{92}Cl_2Cu_6Gd_3N_6O_{24}]^{2+}$

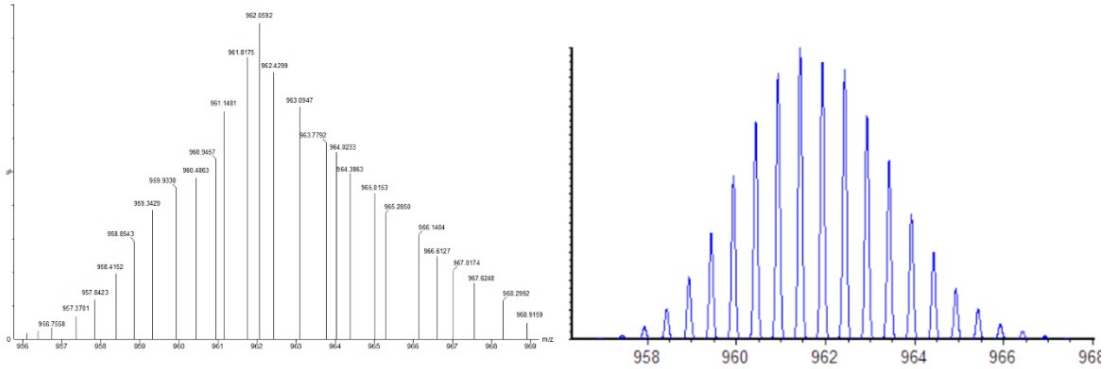

Fig. S11 Simulated and experimental isotope pattern of the prominent peak for $[C_{48}H_{74}Cl_4Cu_5Dy_2N_4O_{27}]^{2+}$.

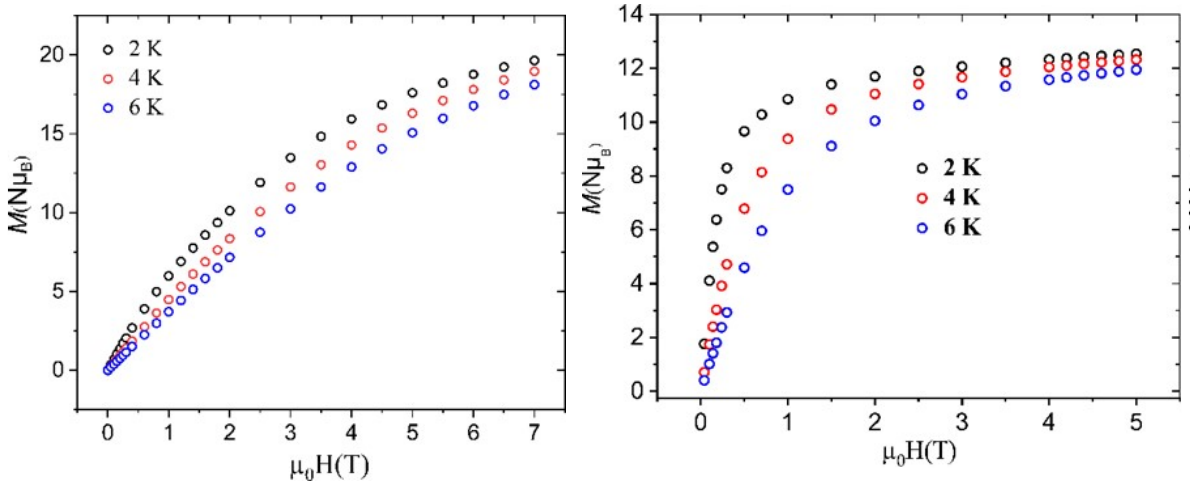

Fig. S12 Magnetisation *vs.* field data for **1** (left) and **2** (right) at 2, 4 and 6 K.

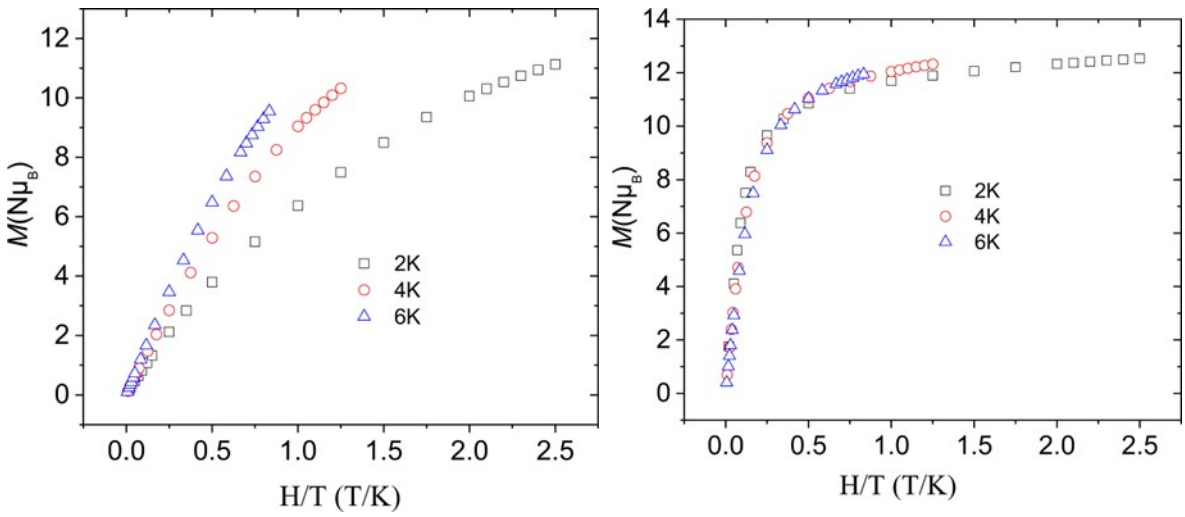

Fig. S13 Reduced magnetisation vs. field data for **1** (left) and **2** (right) at 2, 4 and 6 K.

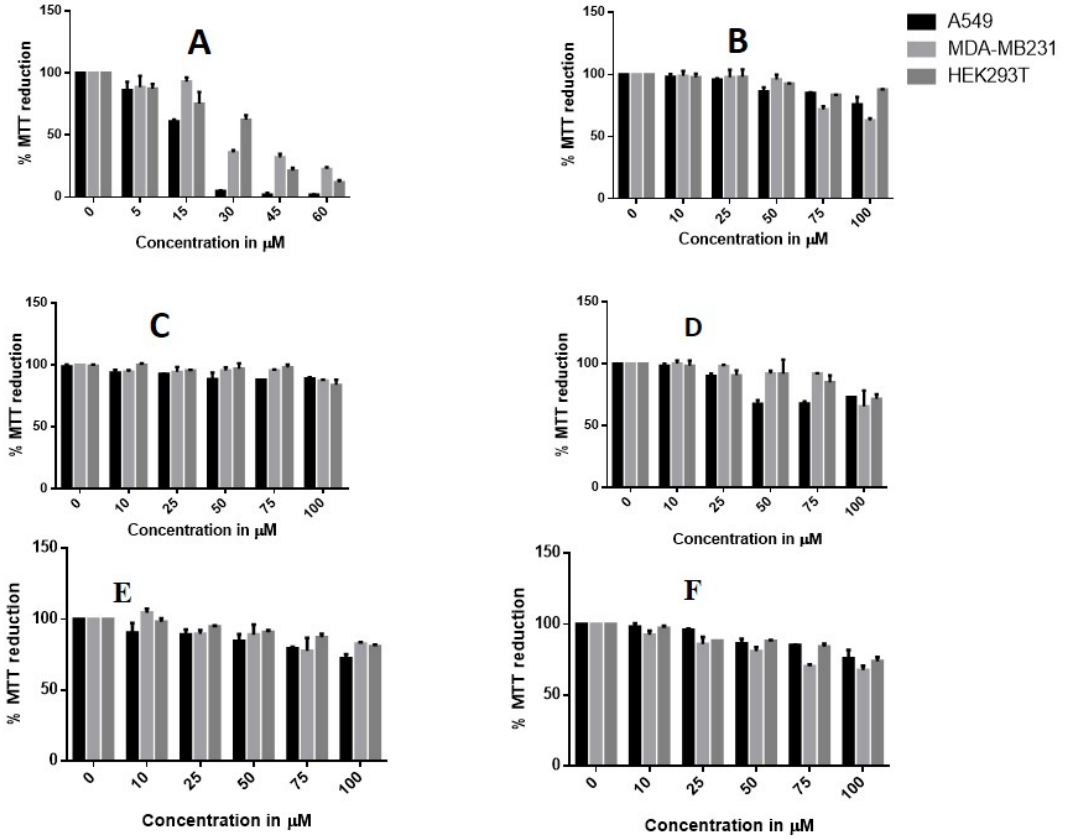

Fig. S14 Percentage of cell growth as a function of **1** (A), **2** (B), Ligand H_2L (C), $Cu(ClO_4)_2 \cdot 6H_2O$ (D), $DyCl_3 \cdot 6H_2O$ (E) and $GdCl_3 \cdot 6H_2O$ (F) concentration for A549 cells (black bars), MDA-MB231 cells (light grey bars) and HEK293T (dark grey bars). The experimental number of cells counted was normalized so that the average of all control experiments was considered as 100 %. At least three independent experiments were performed on different days.

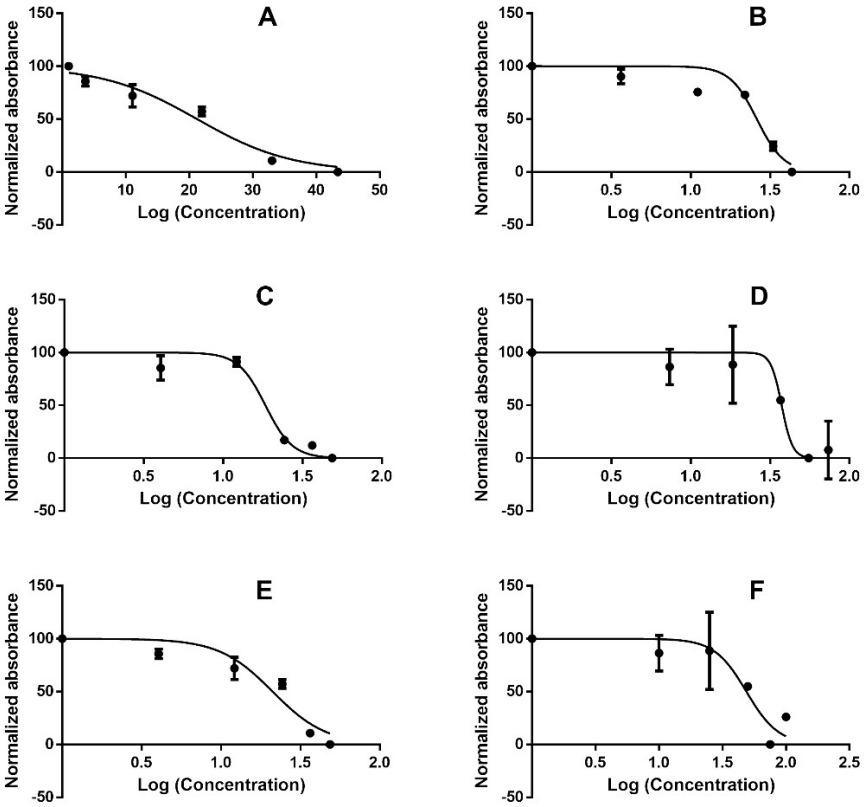

Fig. S15 Cytotoxic effects of **1** and **2** on A549 (A and B), MD-MB-231 (C and D), HEK293 (E and F) cell lines respectively after 24 h exposure, as assessed by the MTT-dye reduction assay. Each data point represents the mean value.

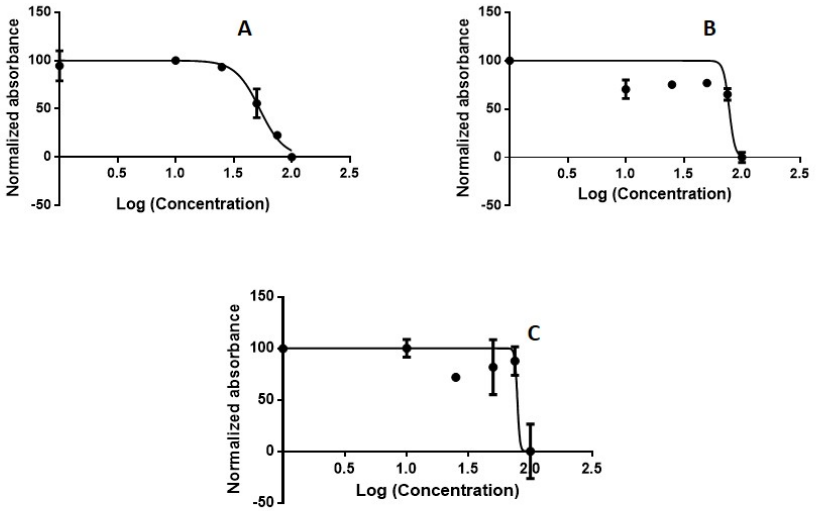

Fig. S16 Cytotoxic effects of ligand H_2L on A549 (A), MD-MB-231 (B) and HEK293 (C) cell lines respectively after 24 h exposure, as assessed by the MTT-dye reduction assay. Each data point represents the mean value.

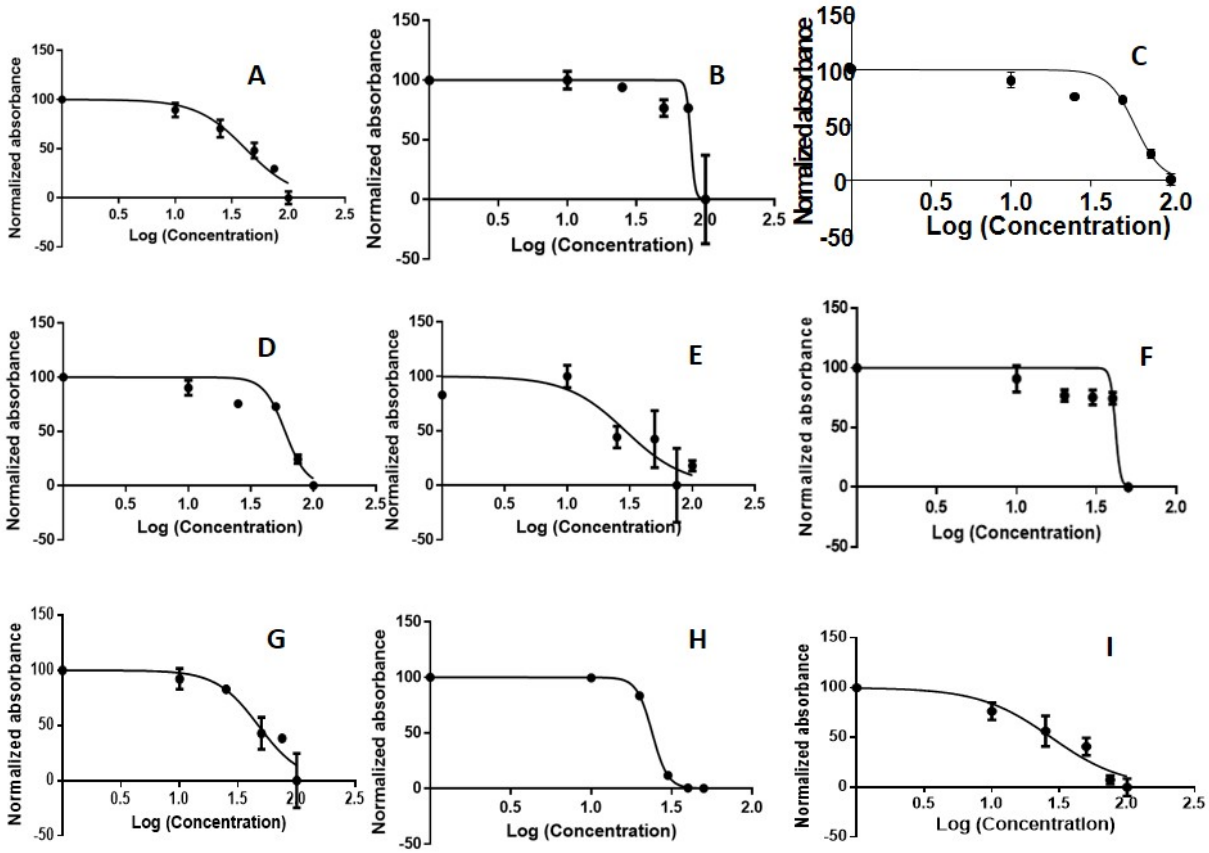

Fig. S17 Cytotoxic effects of starting metal ion precursors $Cu(ClO_4)_2 \cdot 6H_2O$, $DyCl_3 \cdot 6H_2O$ and $GdCl_3 \cdot 6H_2O$ on A549 (A, D, G), MD-MB-231 (B, E, H), HEK293 (C, F, I) cell lines respectively after 24 h exposure, as assessed by the MTT-dye reduction assay. Each data point represents the mean value.

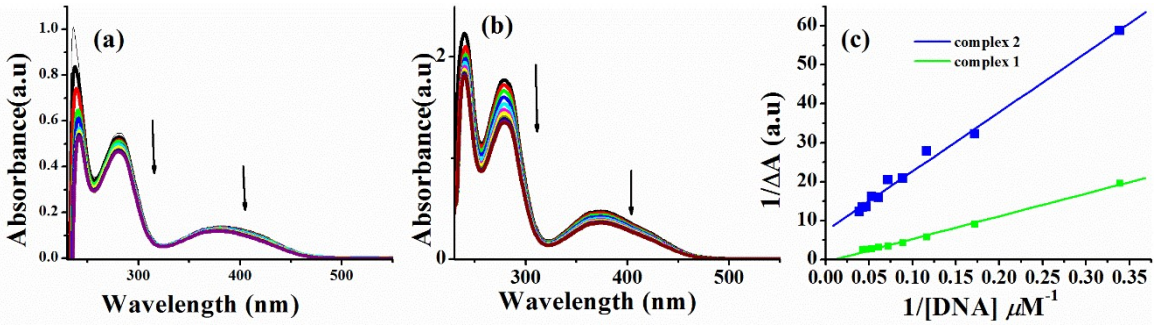

Fig. S18 Absorption spectra of (a) **1** and (b) **2** (25 μM) in the absence and presence of incremental *ct*-DNA (0–50 μM) in 5mM Tris-HCl buffer (50 mMNaCl, *pH* 7.4; (c) Benesi–Hildebrand double reciprocal plot for these complexes.

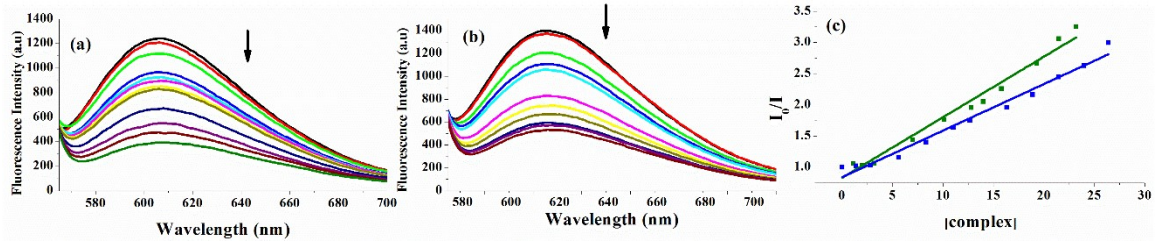

Fig. S19 Emission spectra (λ_{ex}=546 nm) of EtBr-DNA in Tris-HCl buffer in absence and presence of (a) **1** and (b) **2**. The arrow shows the decrease on an intensity of EtBr-DNA upon increasing the concentration of the complexes from 0 to 33 μM. (c) Stern-Volmer plot for complexes **1** and **2**.

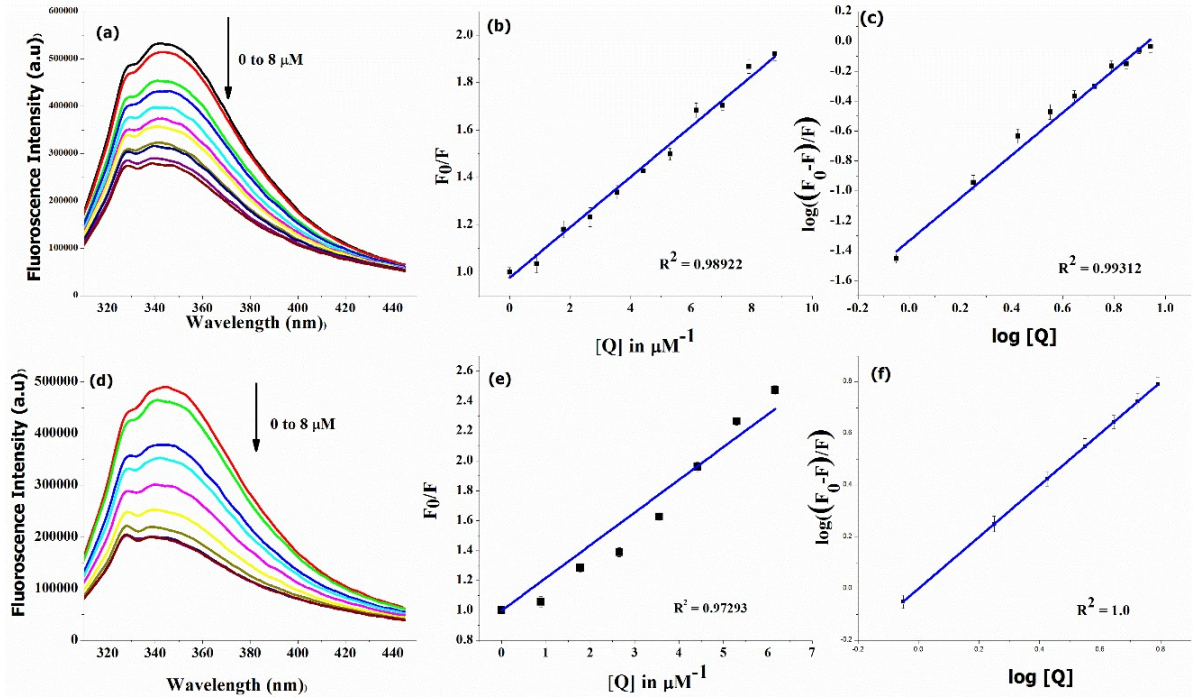

Fig. S20 (a and d) Fluorescence emission spectra of HSA (2 µM) in the absence (top most line) and presence of different concentrations (0 to 8 µM) of 1 and 2, respectively, in 10 mM phosphate buffer of pH 7.4 at 298 K; (b and e) Stern–Volmer and (c and f) double logarithmic plots of **1** and **2**, respectively.

Table S13. Percent decrease in fluorescence intensity of HSA (2.0×10^{-6} M) after addition of 14 μM of quencher complexes

Complexes	% decrease
1	60.2
2	48.2

References

S1. B. S. Furniss, A. J. Hannaford, P. W. G. Smith, A. R. Tatchell, Vogel's Text book of Practical Organic Chemistry, 5th ed.; ELBS, Longman: London, U.K., 1989.

S2. *SAINT, SMART and XPREP*, Siemens Analytical X-ray Instruments Inc., Madison, WI, 1995.

S3. G. M. Sheldrick, SHELXS-2014, Program for Crystal Structure Solution, University of Göttingen, 2014.

S4. G. M. Sheldrick, *Acta Crystallogr., Sect. A: Found. Crystallogr*., 2008, **64**, 112−122.

S5. L. J. J. Farrugia, *WinGX-Version 2014.1*, *Appl. Crystallogr*., 2012, **45**, 849−854.

S6. G. M. Sheldrick, SADABS Software for Empirical AbsorptionCorrection, University of Göttingen, Institute fur AnorganischeChemiederUniversitat, Göttingen, Germany, 1999-2003.

S7. O. V. Dolomanov, L. J. Bourhis, R. J. Gildea, J. A. K. Howard and H. J. Puschmann, *J. Appl. Cryst*., 2009, **42**, 339−341.

S8. DIAMOND, Visual Crystal Structure Information System, version 3.1, Crystal Impact: Bonn, Germany, 2004.

S9. M. E. Reichmann, S. A. Rice, C. A. Thomas and P. Doty, *J. Am. Chem. Soc*., 1954, **76**, 3047–3053.

S10. H. A. Benesi and J. H. Hildebrand, *J. Am. Chem. Soc*., 1949, **71**, 2703–2707.

S11. J. R. Lakowicz, Principles of Fluorescence Spectroscopy, Springer Publishers, New York, third edn, 2006

S12. G. Scatchard, Ann. N. Y. *Acad. Sci*., 1949, **51**, 660–672.

S13. Z.-Y. Li, Y.-X. Wang, J. Zhu, S.-Q. Liu, G. Xin, J.-J. Zhang, H.-Q. Huang and C.-Y. Duan, *Cryst. Growth Des*. 2013, **13**, 3429–3437.

S14. J.-L. Liu, W.-Q. Lin, Y.-C. Chen, S. Gómez-Coca, D. Aravena, E. Ruiz, J.-D. Leng and M.-L. Tong, *Chem.-Eur. J.* 2013, **19**, 17567–17577.

S15. A. Dey, S. Das, M. A. Palacios, E. Colacio and V. Chandrasekhar, *Eur. J. Inorg. Chem*., 2018, 1645–1654.

S16. K. Wang, Z.-L. Chen, H.-H. Zou, Z. Zhang, W.-Y. Sun and F.-P. Liang, *Cryst. Growth Des*., 2015, **15**, 2883–2890.

S17. X. Wang, C. Li, J. Sun and L. Li, *Dalton Trans*., 2015, **44**, 18411–18417.

S18. P. Richardson, K.J. Gagnon, S.J. Teat, G. Lorusso, M. Evangelisti, J. Tang and T.C. Stamatatos, *Cryst. Growth Des*., 2017, **17** 2486–2497.

S19. S. K. Langley, N. F. Chilton, B. Moubaraki, T. Hooper, E.K. Brechin, M. Evangelisti and K.S. Murray, *Chem. Sci.*, 2011, **2**, 1166–1169.

S20. S. K. Langley, B. Moubaraki, C. Tomasi, M. Evangelisti, E. K. Brechin and K. S. Murray, *Inorg. Chem.*, 2014, **53**, 13154–13161.

S21. G. Xiong, H. Xu, J.-Z. Cui, Q.-L. Wang and B. Zhao, *Dalton Trans*., 2014, **43** 5639–5642.

S22. T. N. Hooper, J. Schnack, S. Piligkos, M. Evangelisti and E. K. Brechin, *Angew.Chem. Int. Ed.,* 2012, **51** 4633–4636.

S23. D. I. Alexandropoulos, L. Cunha-Silva, J. Tang and T. C. Stamatatos, *Dalton Trans*., 2018, **47**, 11934–11941.

S24. M. K. Singh, T. Rajeshkumar, R. Kumar, S. K. Singh, G. Rajaraman, *Inorg. Chem*., 2018, **57**, 1846–1858.

S25. R. A. Coxall, S. G. Harris, D. K. Henderson, S. Parsons, P. A. Tasker, R. E. P. Winpenny, *J. Chem. Soc. Dalton Trans*., **2000**, 2349–2356.

S26. M. Pinsky and D. Avnir, *Inorg. Chem*., 1998, **37**, 5575–5582.

S27. D. Casanova, M. Llunell, P. Alemany and S. Alvarez, *Chem. Eur. J*., 2005, **11**, 1479–1494.